



ELSEVIER

Contents lists available at ScienceDirect

Additive Manufacturing

journal homepage: www.elsevier.com/locate/addma

Research Paper

Hot isostatic pressing in metal additive manufacturing: X-ray tomography reveals details of pore closure

A. du Plessis^{a,b,*}, E. Macdonald^c^a Research Group 3DInnovation, Stellenbosch University, Stellenbosch, 7602, South Africa^b Department of Mechanical Engineering, Nelson Mandela University, Port Elizabeth, 6001, South Africa^c Center for Advanced Manufacturing, Youngstown State University, OH 44555, United States

ARTICLE INFO

Keywords:

Metal additive manufacturing
Laser powder bed fusion
Hot isostatic pressing
X-ray tomography
Porosity
Quality control

ABSTRACT

Hot isostatic pressing (HIP) of additively manufactured metals is a widely adopted and effective method to improve the density and microstructure homogeneity within geometrically-complex metal structures fabricated with laser powder bed fusion (LPBF). The role of pores in the fatigue performance of additively manufactured metal parts is increasingly being recognized as a critical factor and HIP post-processing is now heralded as a method to eliminate pores, especially for high-criticality applications such as in the aerospace industry. Despite the widely reported positive influence on fatigue performance and high efficiency of pore closure, examples have been reported in which pores have not been entirely closed or have subsequently re-opened upon heat treatment. A variety of porosity distributions and types of pores may be present in parts produced by LPBF and the effectiveness of pore closure may differ depending on these pore characteristics. In this work, X-ray tomography was employed to provide insights into pore closure efficiency by HIP for an intentional and artificially-induced cavity as well as for a range of typical process-induced pores (lack of fusion, keyhole, contour pores, etc.) in coupon samples of Ti6Al4V. The same samples were imaged non-destructively before and after HIP and aligned carefully for side-by-side viewing. High pore closure efficiency is demonstrated for all types of cavities and pores investigated, but near-surface pores of all types are shown to be problematic to varying degrees, in some cases perforating the superficial surface and creating new external notches. Subsequent heat treatments (annealing after HIP) in some cases resulted in internal pore reopening for previously closed internal pores as well as a new “blistering” effect observed for some near-surface pores, which the authors believe is reported for the first time. Implications of these results for quality control and HIP processing of LPBF parts are discussed. Finally, the utility of using HIP to consolidate intentionally-unmelted powder in order to improve production rates of powder bed fusion has great potential and is preliminarily demonstrated.

1. Introduction

Laser powder bed fusion (LPBF) is a widely used form of additive manufacturing allowing high quality complex geometries to be produced directly from a 3D design in various metal alloys and polymers [1,2]. LPBF technology is increasingly developed for - and adopted by - various industries for the production of critical end-use components [3]. Dramatic advantages exist when compared to traditional manufacturing, including relatively low costs for small lot sizes, short production times and greatly increased geometrical complexity enabling new functionalities [4]. Complexity is particularly of interest for the aerospace industry as considerable light-weighting is possible for functional and load-bearing parts [5–7] through functionally-graded lattices and topology optimization for example. Despite the manifest

potential of the technology and the ever-widening adoption, challenges remain such as quality control, qualification of processes and parts, manufacturing constraints and post processing, among others [8–11].

When considering quality control, the primary concern is the presence of pores or defects (porosity) and different forms of porosity may occur due to unoptimized process parameters, scan strategies, powder feedstock properties, and other parameters, many of which can affect the stability of the track-by-track, layer-by-layer build process. Many widely-known forms of porosity have been identified such as lack-of-fusion pores, metallurgical or gas pores and keyhole pores, all having mainly random distributions within the volume of a part [12]. Localized distributions of porosity are possible; with excessive lack of fusion alongside and between scan tracks and between layers; at the overlap between contour tracks and hatch (infill) tracks; or at the upskin or

* Corresponding author at: Research Group 3DInnovation, Stellenbosch University, Stellenbosch, 7602, South Africa.

E-mail address: anton2@sun.ac.za (A. du Plessis).

<https://doi.org/10.1016/j.addma.2020.101191>

Received 20 February 2020; Received in revised form 17 March 2020; Accepted 29 March 2020

Available online 29 April 2020

2214-8604/ © 2020 The Authors. Published by Elsevier B.V. This is an open access article under the CC BY-NC-ND license

(<http://creativecommons.org/licenses/by-nc-nd/4.0/>).

downskin surfaces where process parameters are generally modified to enhance the surface quality.

Despite the best optimization, the presence of small pores in parts produced by LPBF is inevitable and well known. Pores have been well characterized by X-ray tomography, both in research studies as well as in routine industrial inspection of parts [13]. As an example, a round robin test whereby seven different LPBF laboratories were tasked to produce the same part, demonstrated the widespread occurrence of different porosity types, even while the density of the coupons were more than 99.98% in all cases [14]. Despite the small quantity of pores in optimized processes, pores may influence the mechanical properties of the overall structure and in particular may lead to premature failure in cyclic loading conditions.

The role of pores on the mechanical properties of additively manufactured parts is increasingly recognized, especially in recent years using X-ray tomography to image samples with pores before and after mechanical testing, which improves the understanding of the “effect of defects” [15]. Pores are understood to act as crack initiators in cyclic loading, which may cause premature failure and are likely a major contributor to the wide distribution in fatigue properties reported in various studies as summarized in the review [16].

Hot isostatic pressing (HIPping) is a process whereby a part is subjected to high temperature and confining gas pressure simultaneously. The method has been used for many years in powder metallurgy and cast metals, for the solidification, pore closure and microstructure homogenization of various metals [17] and provides a beneficial effect on the mechanical properties of various metals, demonstrated to effectively close pores up to 5 mm in diameter in cast samples of Ti6Al4V [18]. It has been used to form components in near net shape directly [19,20] and has been demonstrated in a hybrid additive manufacturing process [21].

HIPping has been demonstrated to close porosity in AM materials (both electron beam and laser powder bed fusion) in [22] resulting in improved fatigue performance. Due to the beneficial properties of reducing porosity and homogenizing the microstructure - improving fatigue performance, HIPping has been widely accepted and is used as a crucial process in the production chain of additively manufactured parts for aerospace applications [11,23–25].

Despite this success, HIPping does not always work uniformly well, demanding further study. The HIP parameters must be chosen appropriately for the material (e.g. if the pressure is not high enough for the given material, the pores will not close). Importantly, any pores connected to the surface (even through cracks) will not be closed due to the penetration of confining gas into these open pores during the HIP process. Only pores with sufficient distance from the exterior surface are effectively closed.

X-ray tomography provides a useful insight in this regard. X-ray tomography of powder bed fusion samples before and after HIP processing have identified the extent of porosity reduction with varying results in different studies. In a study by Seifi et al. [26], small random porosity in EBM-produced samples of Ti48Al2Cr2Nb were imaged by X-

ray tomography as small as 20 μm in diameter, and after HIPping, were entirely closed beyond the resolution of the instrument. In the study of a complex Ti6Al4V part produced by LPBF in [27], some pores were closed and others remained unchanged, which was speculated as being due to the unchanged pores being connected to the surface due to the defect being planar (lack of fusion across build plane). Using coupon samples with varying porosity distributions the effectiveness of pore closure was demonstrated in [28], showing how surface-connected pore networks remain unchanged while other pores are entirely closed below the resolution used (24 μm). In a study of LPBF of IN718 [29], it was shown that some pores were not effectively closed by HIP. It was speculated that HIP simply did not close all pores, but the samples were 1.5 mm in thickness so all pores in these samples can be considered “near-surface” and it could likely be that some pores were connected to the surface through cracks invisible to the microCT scans used.

In a study of electron-beam-melted Ti6Al4V, X-ray tomography demonstrated how all pores in the feedstock powder and the final parts were closed by HIPping, but subsequent heat treatment re-opened some of the pores [30]. A detailed study of the re-opening (regrowth) of pores due to a heat treatment after HIP was also reported in [31], which showed how irregular pores closed by HIP remained closed but some small gas pores were re-opened. The reopening was explained as being due to the small gas pores originating from argon atomized powder, while the irregular pores were produced during electron beam melting under vacuum, indicating that the HIP treatment does not fully close gas-containing pores. This phenomenon was studied in [32] for gas-containing pores and hypothesized that higher pressure inside smaller gas-containing pores during HIP processing may improve the solubility of Ar.

Understanding of the efficiency of HIP for different pore types and distributions typical in the context of LPBF is necessary in order to optimize the HIP process and develop an understanding of ultimate limits of the technique. This work focuses on 5.0 mm cubes of Ti6Al4V produced by LPBF which were subjected to high resolution non-destructive microCT imaging before and after HIP. Samples include a cube with intentionally designed cavity, as well as cubes with a range of different typical process-induced porosity distributions. Careful alignment of images allows detailed inspection of changes in samples due to the HIP process.

2. Methods

A series of 5 mm cubes of Ti6Al4V (ELI) were manufactured using an EOS M290 system (using EOS supplied powder) located at Executive Engineering near Cape Town, South Africa. A prior study of process parameter variations for 5.0 mm cubes was performed and the same cubes were used for the HIP processing study reported here, therefore more details of the sample production can be found in [33]. In addition, a cube with an intentionally-designed spherical cavity of 2.0 mm diameter is included in this work. The samples are summarized in Table 1 below, including the most important process parameters.

Table 1
Summary of cubes used in this study.

Description	Power (W)	Speed (mm/s)	Hatch spacing (mm)	Layer height (mm)	Hatch-contour offset (mm)
Artificial 2.0 mm spherical cavity	280	1200	0.14	0.03	0.015
Excessive lack of fusion	90	800	0.14	0.03	0.015
Lack of fusion	120	800	0.14	0.03	0.015
Optimal parameters	160	800	0.14	0.03	0.015
Keyhole pores	360	800	0.14	0.03	0.015
Lack of fusion layer height	280	1200	0.14	0.06	0.015
Lack of fusion hatch width	280	1200	0.23	0.03	0.015
Contour pores	280	1200	0.14	0.03	0.15

X-ray tomography was performed at the Stellenbosch CT facility [34], using a GE Nanotom S System with voltage and current set to 140 kV and 130 μ A, using a 0.5 mm copper beam filter and achieving 5.0 μ m voxel size. The use of X-ray tomography in additive manufacturing has been described in detail in [13]. Image analysis was performed in Volume Graphics VGSTUDIO MAX 3.3, in this case before-after scan data was aligned to allow direct comparison of individual pores side by side in cross-sectional images. Defect analysis was performed using the method described in [35] using a custom defect mask method to minimize user influence. The 3D representation of the defect analysis shows the overall reduction in porosity, while quantitative values were recorded from the defect analysis results.

Hot isostatic pressing was performed at KittyHawk Products Inc (California), using the routine parameter set for Ti6Al4V for all samples in this work. Selected samples were additionally subjected to post-HIP annealing heat treatment at 900 °C for a hold time of 3 h, at Central University of Technology (South Africa).

3. Results and discussion

The cube with an artificial cavity of 2.0 mm in diameter in the middle of a 5.0 mm cube is shown in Fig. 1, before and after HIP. The same cube is aligned carefully to show corresponding features on the surface, and clearly no internal cavity is present after HIP at the scan resolution of 5 μ m, indicating the efficiency of HIPping in closing all internal pore spaces and consolidating all metal powder inside the cavity. The 3D image shows no presence of any pore spaces in the region of the cavity after HIP, at the scan resolution of 5 μ m. Some isolated near-surface pores (black dots) can be seen post-HIP in Fig. 1(a) and these are shown in blue in 3D in Fig. 1(b). A small amount of localized deformation is seen when visualizing the differences between before and after images in Fig. 1(c), showing shrinkage of approximately 30 μ m in the middle of side and bottom surfaces (blue regions).

This inefficiency to close all pores near the surface can be explained by these pores being connected to the surface. In the case of these near-the-surface pores, the argon gas penetrates the cavity and there is no consolidation force acting on the pore, reducing the effectiveness of pore closure. The total closure and consolidation of the large powder-filled cavity is impressive as this is much larger than any typical LPBF defect. In fact, the results highlight the potential utility of this methodology to increase productivity of the LPBF process. If internal volumes are left unmelted in the design, laser time can be conserved, and subsequent HIPping (required for general pore reduction) can be leveraged to simultaneously consolidate the unmelted interior. Further study is required, but this first demonstration is very promising. By incorporating trapped-powder interior cavities, profound benefits can be achieved by reducing production times for many fabricated geometries. Designs which trap unmelted powder within internal cavities can reduce the amount of hatch scan melting required to fabricate the part. A subsequent HIP step (required regardless for reducing general porosity) could be exploited to avoid substantial selective laser melting, and consequently, to improve the production rate of powder bed fusion.

In order to evaluate the efficiency of the HIP processing on typical LPBF porosities (less extreme than the 2.0 mm artificial cavity above), a series of process-induced porosity examples are used. Since different porosity types have different shapes and connectivity, the efficiency of the HIP process was expected to vary. In a previous study, 5.0 mm cubes were produced at different process parameters with variations from optimal process parameters. This includes variation of laser power, while keeping all other parameters at optimal values such as the hatch spacing and layer height. The resulting porosity was characterized in detail by microCT, with results shown in Fig. 2, modified from [33]. The four indicated examples (a)–(d) were selected for this study for HIP processing. Example (a) is excessive lack of fusion; (b) is simple lack of fusion; (c) is optimal for this scan speed resulting in 99.99%

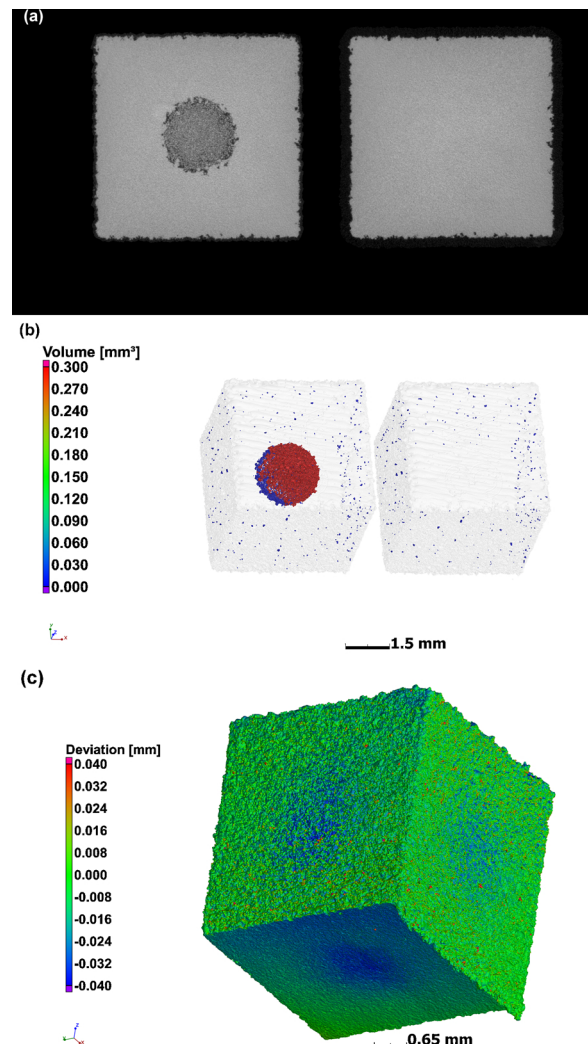


Fig. 1. The same cube with an artificially designed spherical cavity imaged before and after HIP, showing how metal powder is consolidated and no pores larger than 5 μ m remain after HIP in the centre of the cube. (a) cross sectional slice image (left = before HIP, right = after HIP), (b) shows 3D view with defect analysis applied to pore spaces (left = before HIP, right = after HIP), (c) deformation map showing localized shrinkage in middle of side and bottom surfaces due to HIP. (For interpretation of the references to colour in this figure legend, see the color plate.)

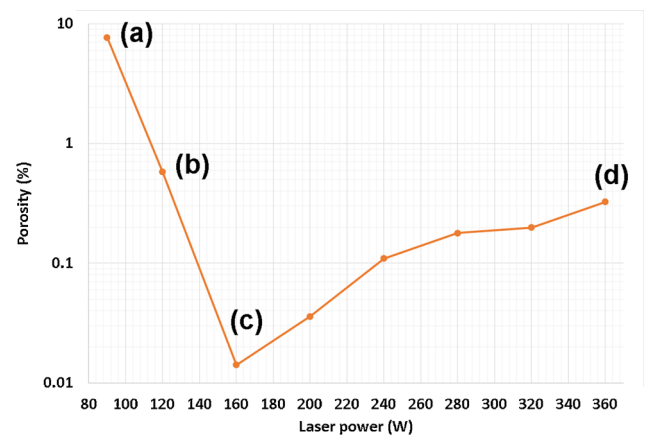


Fig. 2. Varying porosity as a function of laser power, indicating the examples used in this work for further HIP processing: (a) is excessive lack of fusion; (b) is normal lack of fusion; (c) is optimal parameter set; (d) is keyhole mode porosity regime.

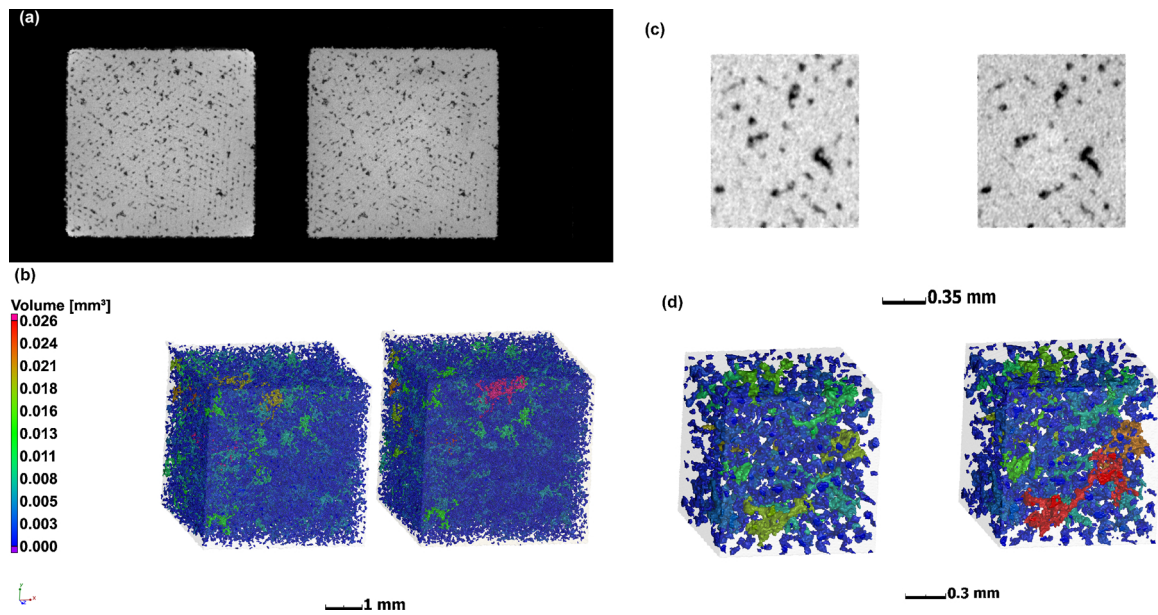


Fig. 3. High porosity due to excessive lack of fusion at low laser power, before and after HIP (left and right in each case) showing in (a) CT slice image of entire 5 mm cube before and after HIP, (b) 3D image of entire 5 mm cube with colour coded porosity before and after HIP, (c) 1.2 mm selected region in centre of cube in slice images before and after HIP and (d) 3D image of 1.2 mm central section before and after HIP.

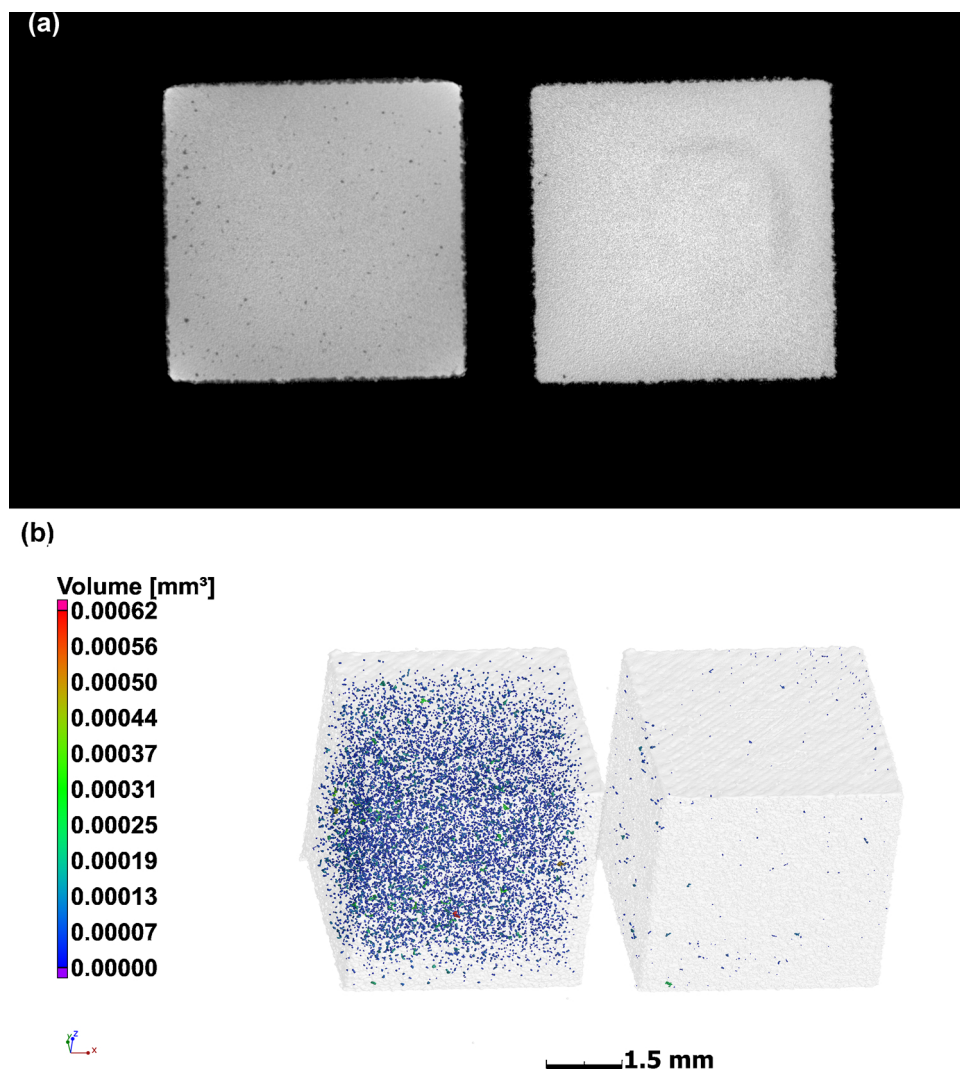


Fig. 4. Porosity at 0.6% due to lack of fusion at low power, before and after HIP (left and right in each case). Almost all pores are closed, except a small number near the surface – presumably connected to the surface.

density; and (d) is high power resulting in keyhole mode pores. Each of these examples is described separately below.

The lowest power of 90 W at this parameter set for 800 mm/s scan speed causes an excessively high porosity in the region of 8%. As seen in Fig. 3, this porosity is highly interconnected and hence connected to the surface, rendering the HIP process mostly ineffectual. Close inspection of the images in Fig. 3 indicates that some small isolated pores are closed by HIP and that interconnected pore spaces may potentially increase in connectivity (larger connected pore spaces in post-HIP images). This could potentially be explained by narrow pore connections being opened by the high pressure gas penetration.

The next example at 120 W power has 0.6% porosity randomly distributed in the sample prior to HIP and almost all of these pores are closed in the HIP process as seen in Fig. 4. No pores remain in the

middle of the same and only some isolated pores near the surface are observed after HIP. The efficiency of the HIPping is high in this case.

At optimal values of power and scan speed, approximately 0.01% porosity is present in the samples prior to HIP. The post HIP images in Fig. 5 show no pores remain. As less pores are present before HIP, the likelihood for near-surface pores reduces, which results in no observed cases of near-surface pores after HIP (none unaffected by HIP). This is one major result of the reported work: a combination of optimal process parameters + HIP is the best solution for full density parts.

Keyhole mode porosity is often present in parts where the power is set too high or scan speed is too low: these pores are rounded in shape and in the case in Fig. 6, prior to HIP, the porosity is 0.33%. In this

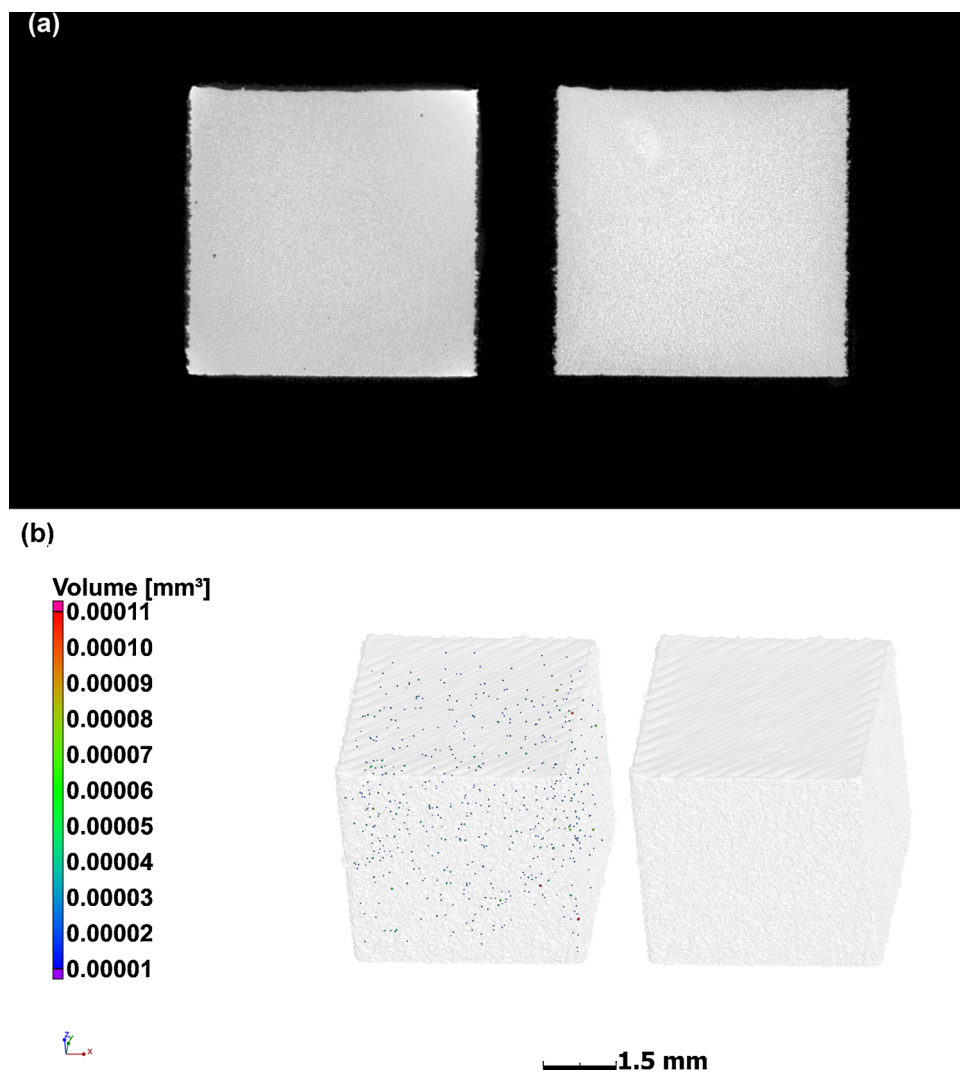


Fig. 5. Ideal process parameters with 0.01% porosity prior to HIP and no pores remaining after HIP, at 5 μm voxel size, before and after HIP (left and right in each case).

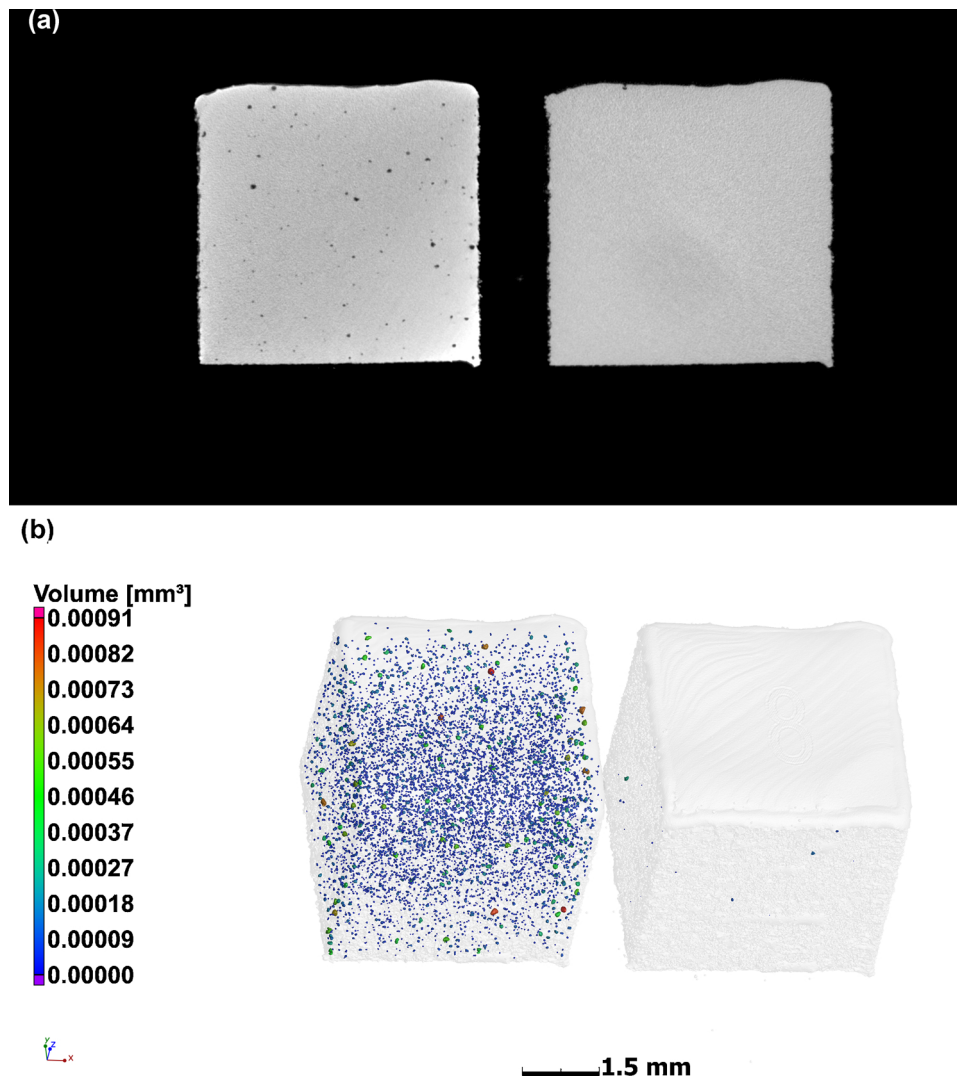


Fig. 6. Keyhole mode pores at 0.33% prior to HIP and only some isolated pores near surface remain, before and after HIP (left and right in each case).

case the majority of pores are closed with the only exceptions being some isolated near-surface pores. This is consistent with the above-mentioned observations.

Additional typical porosity types investigated here were cases of processing with the layer height, hatch spacing and contour-hatch offset values set too high, in each case causing a particular porosity distribution. The layer height selection of 0.06 mm instead of 0.03 mm causes a higher likelihood for lack of fusion in places when the powder layer is not perfectly evenly spread. This is seen in Fig. 7, where it is also shown how all of these pores are closed by HIP in this experiment.

For the case of hatch spacing set to 0.23 mm instead of the nominal 0.14 mm, lack of fusion between tracks was expected. This is shown in Fig. 8 before HIP – and the HIP process is shown to be effective in closing all internal pores in this case as well, with the exception of some surface-connected pore spaces.

Finally, the offset between hatch and contour tracks is nominally set to 0.015 mm for good overlap. In this case, with a 10 times larger setting of 0.15 mm, pores between contour tracks and hatch tracks were induced as shown in Fig. 9. Other causes of near-surface contour pores exist but will not be discussed here in detail. In this case, the HIP process was effective in some cases and not in others – most likely due to the connected nature of the contour pores, with some connection to the surface causing the HIP to be ineffective.

The results demonstrated in the above examples (and summarized in the Table 2), emphasize the importance of porosity not being connected to the surface, for the HIP process to be effective. The careful alignment of the images allowed for the identification of some additional features. In Fig. 10 is shown three examples of near-surface pores which were “opened” by the HIP process, leaving a potentially harmful notch in the surface and degrading the surface finish. The circles highlight individual features of this type in examples of

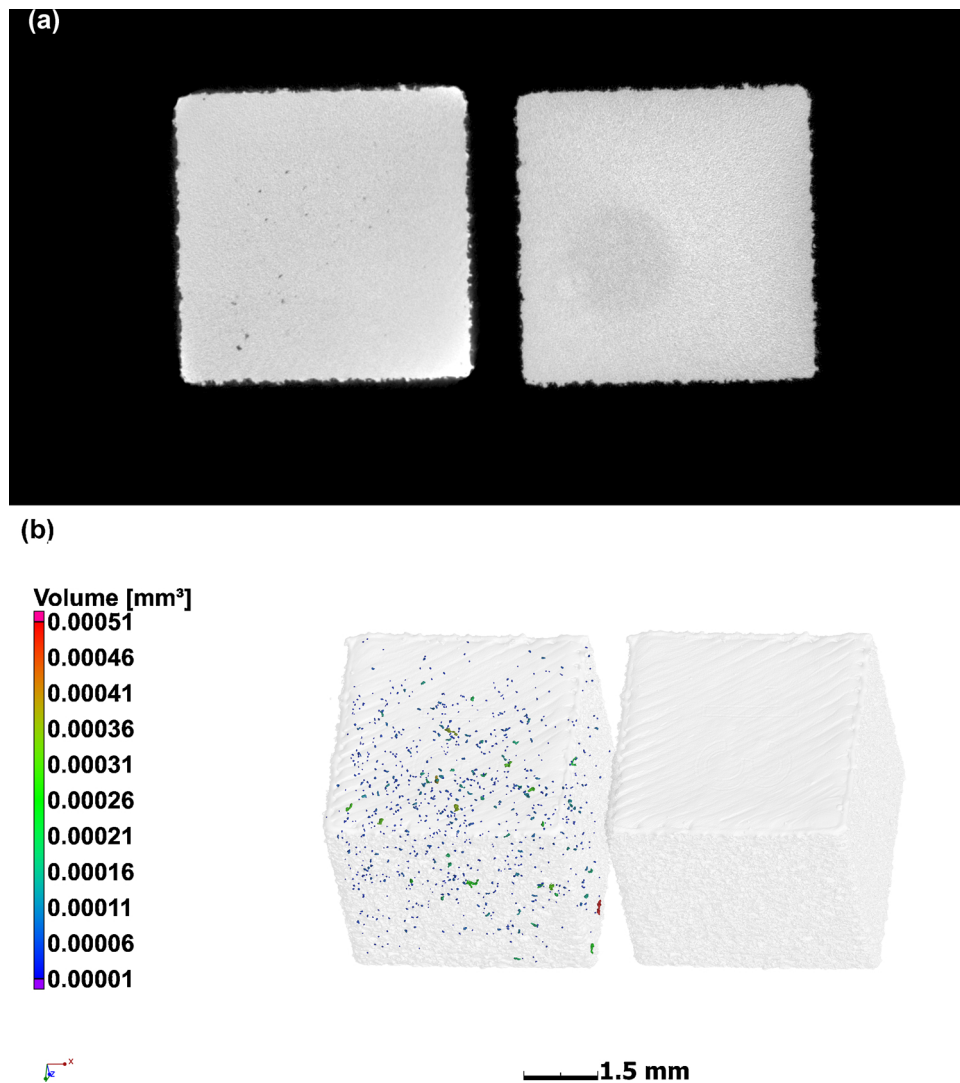


Fig. 7. Layer height at 0.06 mm instead of 0.03 mm creates some lack of fusion pores between layers, all of which are closed by HIP in this case. Before and after HIP (left and right in each case).

keyhole mode porosity (a) and (b) and in the artificial cavity example where no contour tracks were used (c).

Due to preliminary studies indicating the potential for closed gas-containing pores to be re-opened on subsequent heat treatment, an investigation was focused on this for selected examples. In Fig. 11 is shown the 2.0 mm cavity after HIP and subsequent annealing heat treatment – some evidence of pore opening is confirmed. This is presumably not critical for practical applications – as HIP is usually not followed by further heat treatments, but this indicates that the pores are not entirely sealed and exist below the resolution of the scan after HIP (<5 μm). The influence of such small high-gas-pressure pores on mechanical properties of parts requires further investigation, and may well be important for high temperature applications.

Finally, annealing heat treatment of the contour pore samples showed an interesting feature – a blistering effect as shown in Fig. 12. As can be seen to the right of the series of images, a new large pore has formed after HIP + anneal, compared to directly after HIP. The 3D image shows this in a colour-coded view to indicate two cases of this occurring in this sample. One potential explanation of this is that an existing pore was filled by argon gas during HIP processing and then sealed, potentially through a narrow crack which sealed during HIPping, or upon cooling. This high-pressure gas inside a pore near the surface, when subjected to high temperature annealing heat treatment, expands and forces the thin layer of metal on the surface outward, causing a blistering effect. Again, it should be mentioned that this is not expected to be a problem due to heat treatment not

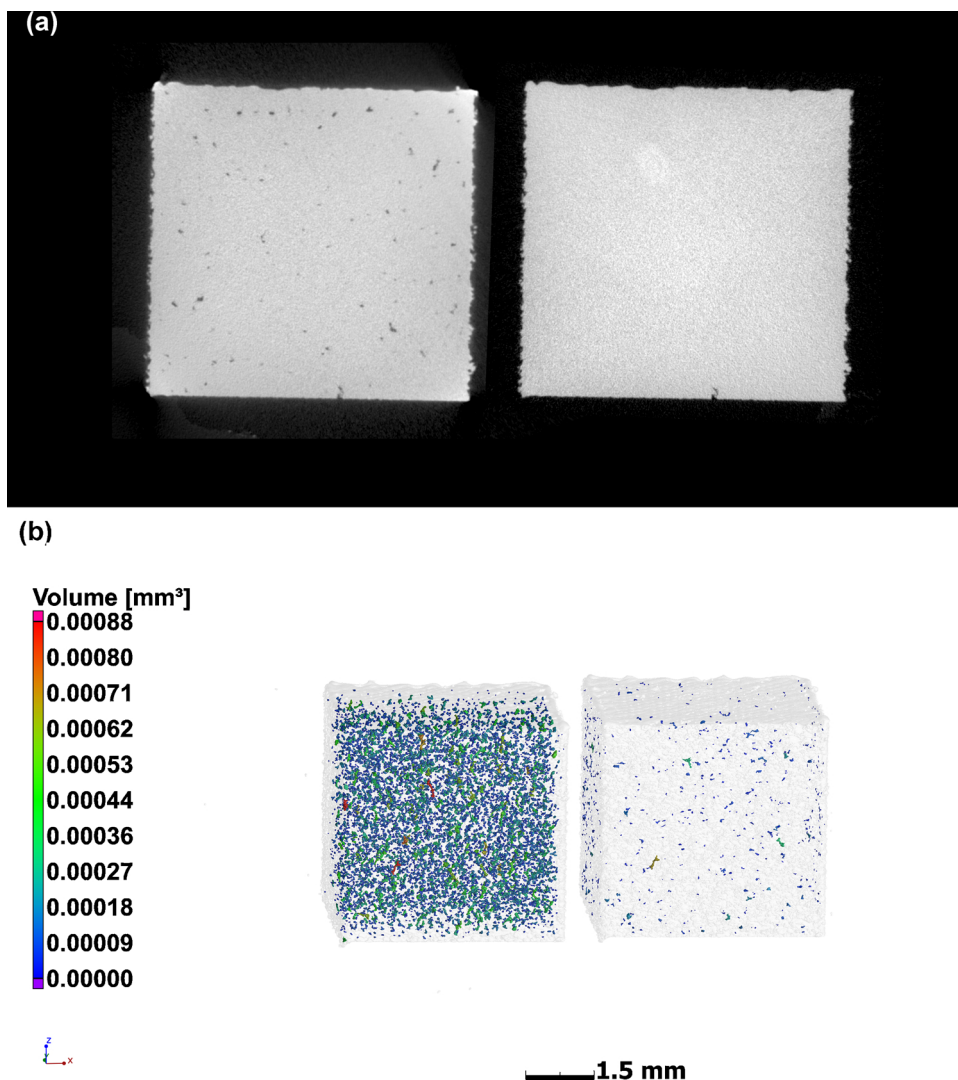


Fig. 8. Hatch spacing set to 0.23 mm instead of nominal 0.14 mm, before and after HIP (left and right in each case).

usually being applied after HIP. However, this may well be a weak point in the structure after HIP alone, due to the high gas pressure sealed inside the pore and this pore located near the surface – a latent problem. As also mentioned above, this effect may be important for high temperature applications.

4. Conclusions

A detailed characterization of HIP efficiency for additively manufactured Ti6Al4V cubes was completed by X-ray tomography. It was shown how HIP is highly effective in closing pores and reducing porosity in all cases, but some variations exist due to the connectivity of pores, the connectivity to the surface and the proximity to the surface. Detailed side-by-side inspection of CT data allowed to highlight some important features, including most notably the HIP process causing a

break-through and opening of near-surface pores in some cases, leaving a surface defect (notch). Poor efficiency of pore closure was shown for excessive lack of fusion, and for excessive contour porosity. All other forms of porosity were closed with high efficiency, with the best result found for samples with initially the lowest porosity: the best solution is optimized LPBF process parameters + HIP. Evidence for pore opening and a blistering effect was observed upon HIP + anneal treatment, indicating some pores near surface may be under high pressure post-HIP.

This study made use of Ti6Al4V and LPBF in particular but the results are expected to be relevant to all metal additive manufacturing broadly. More work remains to establish the importance of pore closure and the effect of near-surface pores on fatigue properties, but the results presented here demonstrate that near-surface pores are not always closed and HIP can be problematic for some of these cases. This

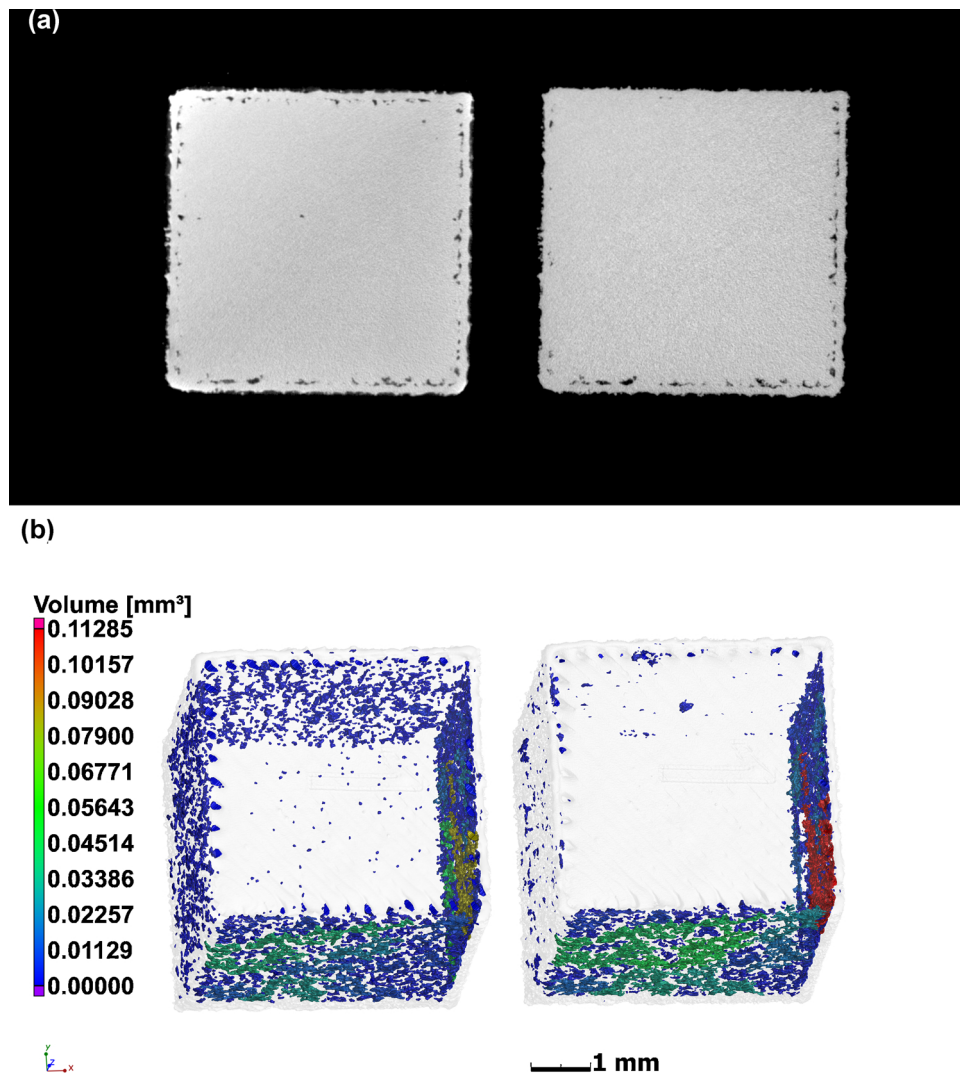


Fig. 9. Contour offset of 0.15 mm instead of 0.015 mm causing extensive connected contour pores, with varied HIP success – some pores are closed while others are not. Before and after HIP (left and right in each case).

Table 2
Summary results of porosity before and after HIP process for each sample type.

Description	Porosity before (%)	Porosity after (%)
Artificial 2.0 mm spherical cavity	0.361	0
Excessive lack of fusion	7.700	6.8
Lack of fusion	0.351	0.0039
Optimal parameters	0.011	0
Keyhole pores	0.298	0.0007
Lack of fusion layer height	0.034	0
Lack of fusion hatch width	0.616	0.0143
Contour pores	0.911	0.643

emphasizes the fact that scan strategy and process parameters should be optimized to minimize these pores in the first place, due to the inefficiency of HIP in closing them. The importance of good contour

scanning is emphasized by the results here, as any internal pores will be sealed by HIP if the contour tracks are fully dense. The combination of optimal parameters and HIP is one good solution. Other methods of closing near-surface pores also exist such as shot peening and laser shock peening [36], but these require access to the surface of interest, so this is not possible inside complex parts such as lattice structures. These results also explain why some studies investigating lattice structures subjected to HIP showed much less pore closure as compared to bulk solid parts – due to all pores being close to surface in this case. Surface roughness and microcracks can likely create connections between these pores and the surface in such structures, making the HIPping less effective.

Finally, these results should be used to further establish safe operating regimes with a holistic optimization of process and scanning strategy (especially with a focus on contour tracks to ensure no near-surface pores), HIPping and non-destructive testing, for a full qualification process of parts for critical applications.

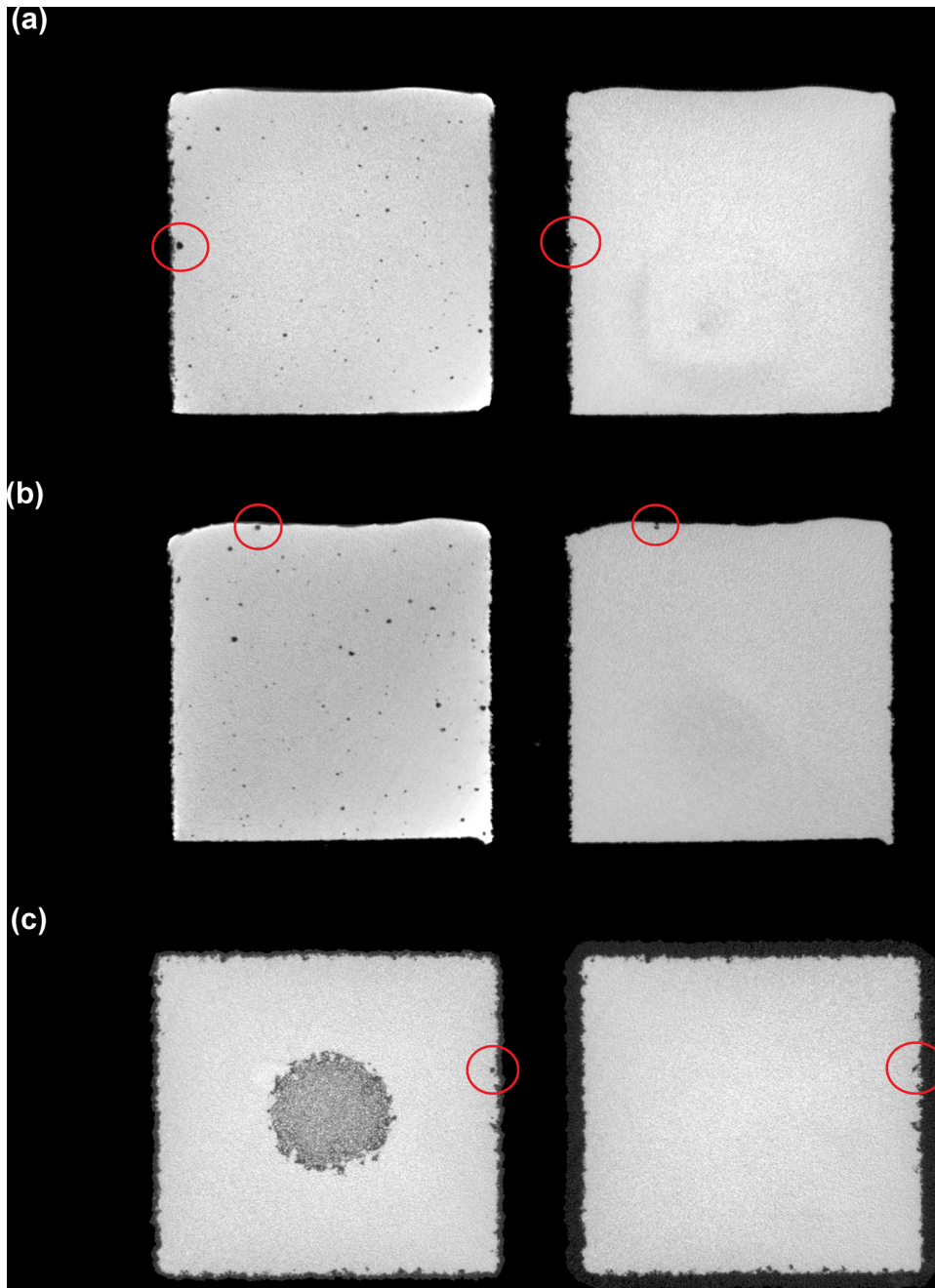


Fig. 10. Examples of near-surface pores which are opened by HIP, creating a new surface notch defect. Before and after HIP (left and right in each case).

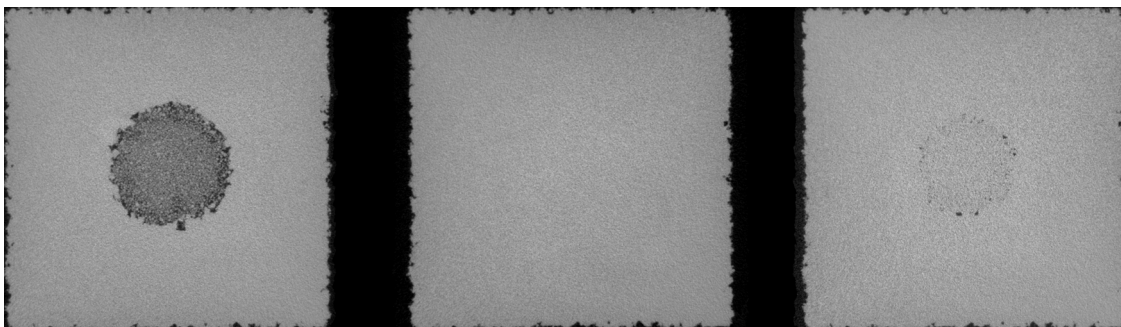


Fig. 11. Spherical cavity with powder before HIP (left), after HIP (middle) and after HIP and subsequent annealing heat treatment (right). Pore regrowth is observed.

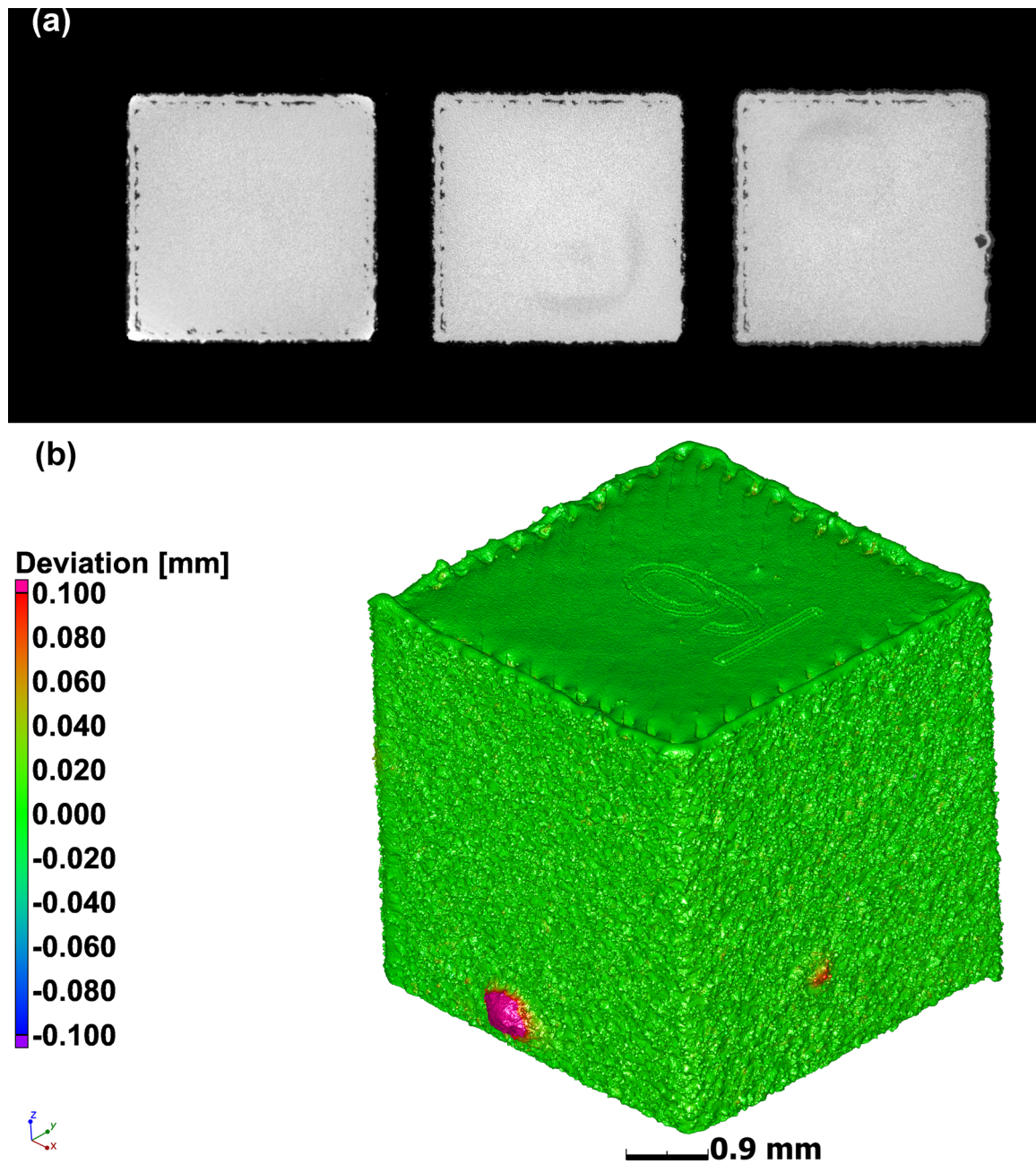


Fig. 12. Blistering effect observed in contour-porosity sample subjected to HIP and subsequent heat treatment.

Declaration of Competing Interest

Both authors of this article are part of the editorial board of the journal. To avoid potential conflicts of interest, the responsibility for the editorial and peer-review process of this article lies with the other editors of the journal. Furthermore, the authors of this article were removed from the peer review process and have no access to confidential information related to the editorial process of this article.

Acknowledgements

The Collaborative Program for Additive Manufacturing (CPAM), funded by the South African Department of Science and Innovation, is acknowledged for financial support. Muofhe Tshibalanganda and Carlyn Wells are thanked for microCT scanning and Dean Kouprianoff is thanked for support in annealing heat treatment. This research was

funded in part by the Morris Friedman Endowment for Manufacturing at Youngstown State University.

References

- [1] T. Debroy, H.L. Wei, J.S. Zuback, T. Mukherjee, J.W. Elmer, J.O. Milewski, A.M. Beese, A. Wilson-Heid, A. De, W. Zhang, Additive manufacturing of metallic components – process, structure and properties, *Prog. Mater. Sci.* 92 (2018) 112–224, <https://doi.org/10.1016/j.pmatsci.2017.10.001>.
- [2] D.D. Gu, W. Meiners, K. Wissenbach, R. Poprawe, Laser additive manufacturing of metallic components: materials, processes and mechanisms, *Int. Mater. Rev.* 57 (2012) 133–164, <https://doi.org/10.1179/1743280411Y.0000000014>.
- [3] T. Wohlers, T. Caffrey, R.I. Campbell, O. Diegel, J. Kowen, *Wohlers Report 2018: 3D Printing and Additive Manufacturing State of the Industry*, (2018).
- [4] A. du Plessis, C. Broeckhoven, I. Yadroitsava, I. Yadroitsev, C.H. Hands, R. Kunju, D. Bhate, Beautiful and functional: a review of biomimetic design in additive manufacturing, *Addit. Manuf.* (2019), <https://doi.org/10.1016/J.ADDMA.2019.03.033>.
- [5] M. Orme, I. Madera, M. Gschweil, M. Ferrari, Topology optimization for additive manufacturing as an enabler for light weight flight hardware, *Designs.* 2 (2018),

- <https://doi.org/10.3390/designs2040051>.
- [6] M.E. Orme, M. Gschweid, M. Ferrari, I. Madera, F. Mouriaux, Designing for additive manufacturing: lightweighting through topology optimization enables lunar spacecraft, *J. Mech. Des.* 139 (2017) 100905, <https://doi.org/10.1115/1.4037304>.
 - [7] E. Uhlmann, R. Kersting, T.B. Klein, M.F. Cruz, A.V. Borille, Additive manufacturing of titanium alloy for aircraft components, *Procedia Cirp* 35 (2015) 55–60, <https://doi.org/10.1016/j.procir.2015.08.061>.
 - [8] T. DehRoy, T. Mukherjee, J.O. Milewski, J.W. Elmer, B. Ribic, J.J. Blecher, W. Zhang, Scientific, technological and economic issues in metal printing and their solutions, *Nat. Mater.* (2019) 1, <https://doi.org/10.1038/s41563-019-0408-2>.
 - [9] A.D. Brandão, R. Gerard, J. Gumpinger, S. Beretta, A. Makaya, L. Pambaguian, T. Ghidini, Challenges in additive manufacturing of space parts: powder feedstock cross-contamination and its impact on end products, *Materials (Basel)*. 10 (2017), <https://doi.org/10.3390/ma10050522>.
 - [10] A. Yadollahi, N. Shamsaei, Additive manufacturing of fatigue resistant materials: challenges and opportunities, *Int. J. Fatigue* 98 (2017) 14–31, <https://doi.org/10.1016/j.ijfatigue.2017.01.001>.
 - [11] M. Seifi, A. Salem, J. Beuth, O. Harrysson, J.J. Lewandowski, Overview of materials qualification needs for metal additive manufacturing, *JOM*. 68 (2016) 747–764, <https://doi.org/10.1007/s11837-015-1810-0>.
 - [12] H. Gong, K. Rafi, H. Gu, T. Starr, B. Stucker, Analysis of defect generation in Ti-6Al-4V parts made using powder bed fusion additive manufacturing processes, *Addit. Manuf.* 1 (2014) 87–98, <https://doi.org/10.1016/j.addma.2014.08.002>.
 - [13] A. du Plessis, I. Yadroitsev, I. Yadroitsava, S.G. Le Roux, X-ray microcomputed tomography in additive manufacturing: a review of the current technology and applications, *3D Print. Addit. Manuf.* 5 (2018), <https://doi.org/10.1089/3dp.2018.0060> 3dp.2018.0060.
 - [14] A. du Plessis, S.G. le Roux, Standardized X-ray tomography testing of additively manufactured parts: a round robin test, *Addit. Manuf.* 24 (2018) 125–136, <https://doi.org/10.1016/j.addma.2018.09.014>.
 - [15] A. du Plessis, I. Yadroitsava, I. Yadroitsev, Effects of defects on mechanical properties in metal additive manufacturing: a review focusing on X-ray tomography insights, *Mater. Des.* 187 (2020), <https://doi.org/10.1016/j.matdes.2019.108385>.
 - [16] J.J. Lewandowski, M. Seifi, Metal additive manufacturing: a review of mechanical properties, *Annu. Rev. Mater. Res.* 46 (2016) 151–186, <https://doi.org/10.1146/annurev-matsci-070115-032024>.
 - [17] H.V. Atkinson, S. Davies, Fundamental aspects of hot isostatic pressing: an overview, *Metall. Mater. Trans. A Phys. Metall. Mater. Sci.* 31 (2000) 2981–3000, <https://doi.org/10.1007/s11661-000-0078-2>.
 - [18] A. du Plessis, P. Rossouw, Investigation of porosity changes in cast Ti6Al4V rods after hot isostatic pressing, *J. Mater. Eng. Perform.* 24 (2015) 3137–3141, <https://doi.org/10.1007/s11665-015-1580-4>.
 - [19] C. Cai, B. Song, P. Xue, Q. Wei, C. Yan, Y. Shi, A novel near α -Ti alloy prepared by hot isostatic pressing: microstructure evolution mechanism and high temperature tensile properties, *Mater. Des.* 106 (2016) 371–379, <https://doi.org/10.1016/j.matdes.2016.05.092>.
 - [20] C. Cai, B. Song, P. Xue, Q. Wei, J.M. Wu, W. Li, Y. Shi, Effect of hot isostatic pressing procedure on performance of Ti6Al4V: surface qualities, microstructure and mechanical properties, *J. Alloys. Compd.* 686 (2016) 55–63, <https://doi.org/10.1016/j.jallcom.2016.05.280>.
 - [21] C. Cai, X. Gao, Q. Teng, M. Li, K. Pan, B. Song, C. Yan, Q. Wei, Y. Shi, A novel hybrid selective laser melting/hot isostatic pressing of near-net shaped Ti-6Al-4V alloy using an in-situ tooling: interfacial microstructure evolution and enhanced mechanical properties, *Mater. Sci. Eng. A*. 717 (2018) 95–104, <https://doi.org/10.1016/j.msea.2018.01.079>.
 - [22] H. Masuo, Y. Tanaka, S. Morokoshi, H. Yagura, T. Uchida, Y. Yamamoto, Y. Murakami, Influence of defects, surface roughness and HIP on the fatigue strength of Ti-6Al-4V manufactured by additive manufacturing, *Int. J. Fatigue* 117 (2018) 163–179, <https://doi.org/10.1016/j.ijfatigue.2018.07.020>.
 - [23] M. Seifi, M. Gorelik, J. Waller, N. Hrabe, N. Shamsaei, S. Daniewicz, J.J. Lewandowski, Progress towards metal additive manufacturing standardization to support qualification and certification, *JOM*. 69 (2017) 439–455, <https://doi.org/10.1007/s11837-017-2265-2>.
 - [24] ASTM F2924-12, Standard specification for additive manufacturing Titanium-6 Aluminum-4 vanadium with powder bed fusion, *ASTM Int.* (2012), <https://doi.org/10.1520/F2924-14>.
 - [25] M. Ahlfors, F. Bahbou, A. Eklund, HIP for AM - optimized material properties by HIP, *Mater. Res. Soc. Symp. Proc.* 10 (2019) 1–10, <https://doi.org/10.21741/9781644900031-1>.
 - [26] M. Seifi, A.A. Salem, D.P. Satko, U. Ackelid, S.L. Semiatin, J.J. Lewandowski, Effects of HIP on microstructural heterogeneity, defect distribution and mechanical properties of additively manufactured EBM Ti-48Al-2Cr-2Nb, *J. Alloys. Compd.* 729 (2017) 1118–1135, <https://doi.org/10.1016/J.JALLCOM.2017.09.163>.
 - [27] A. du Plessis, S.G. le Roux, J. Els, G. Booyens, D.C. Blaine, Application of microCT to the non-destructive testing of an additive manufactured titanium component, *Case Stud. Nondestruct. Test. Eval.* 4 (2015) 1–7, <https://doi.org/10.1016/j.csndt.2015.09.001>.
 - [28] S. Tammas-Williams, P.J. Withers, I. Todd, P.B. Prangnell, The effectiveness of hot isostatic pressing for closing porosity in titanium parts manufactured by selective electron beam melting, *Metall. Mater. Trans. A Phys. Metall. Mater. Sci.* 47 (2016) 1939–1946, <https://doi.org/10.1007/s11661-016-3429-3>.
 - [29] W. Tillmann, C. Schaak, J. Nellesen, M. Schaper, M.E. Aydinöz, K.-P. Hoyer, Hot isostatic pressing of IN718 components manufactured by selective laser melting, *Addit. Manuf.* 13 (2017) 93–102, <https://doi.org/10.1016/J.ADDMA.2016.11.006>.
 - [30] R. Cunningham, A. Nicolas, J. Madsen, E. Fodran, E. Anagnostou, M.D. Sangid, A.D. Rollett, Analyzing the effects of powder and post-processing on porosity and properties of electron beam melted Ti-6Al-4V, *Mater. Res. Lett.* 5 (2017) 516–525, <https://doi.org/10.1080/21663831.2017.1340911>.
 - [31] S. Tammas-Williams, P.J. Withers, I. Todd, P.B. Prangnell, Porosity regrowth during heat treatment of hot isostatically pressed additively manufactured titanium components, *Scr. Mater.* 122 (2016) 72–76, <https://doi.org/10.1016/J.SCRIPTAMAT.2016.05.002>.
 - [32] S. Shao, M.J. Mahtabi, N. Shamsaei, S.M. Thompson, Solubility of argon in laser additive manufactured α -titanium under hot isostatic pressing condition, *Comput. Mater. Sci.* 131 (2017) 209–219, <https://doi.org/10.1016/j.commatsci.2017.01.040>.
 - [33] A. du Plessis, Effects of process parameters on porosity in laser powder bed fusion revealed by X-ray tomography, *Addit. Manuf.* 30 (2019), <https://doi.org/10.1016/j.addma.2019.100871>.
 - [34] A. du Plessis, S.G. le Roux, A. Guelpa, The CT scanner facility at Stellenbosch University: an open access X-ray computed tomography laboratory, *Nucl. Instruments Methods Phys. Res. Sect. B Beam Interact. with Mater. Atoms.* 384 (2016) 42–49, <https://doi.org/10.1016/j.nimb.2016.08.005>.
 - [35] A. du Plessis, P. Sperling, A. Beerlink, L. Tshabalala, S. Hoosain, N. Mathe, G. Stephan, MethodsX Standard method for microCT-based additive manufacturing quality control 1 : porosity analysis, *MethodsX*. 5 (2018) 1102–1110, <https://doi.org/10.1016/j.mex.2018.09.005>.
 - [36] A. du Plessis, D. Glaser, H. Moller, N. Mathe, L. Tshabalala, B. Mfusi, R. Mostert, Pore closure effect of laser shock peening of additively manufactured AlSi10Mg, *3D Print. Addit. Manuf.* 6 (2019), <https://doi.org/10.1089/3dp.2019.0064>.